Journal of Sound and Vibration (2002) **249**(1), 129–145
doi:10.1006/jsvi.2001.3848, available online at http://www.idealibrary.com on IDEAL®

PLANETARY GEAR PARAMETRIC INSTABILITY CAUSED BY MESH STIFFNESS VARIATION

J. LIN

John Deere Product Engineering Center, Waterloo, IA 50704, *U.S.A.*

AND

R. G. PARKER

Department of Mechanical Engineering, The Ohio State University, Columbus, OH 43210, *U.S.A.*
E-mail: parker.242@osu.edu

(*Received* 28 *November* 2000, *and in final form* 21 *June* 2001)

Parametric instability is investigated for planetary gears where fluctuating stiffness results from the changing contact conditions at the multiple tooth meshes. The time-varying mesh stiffnesses of the sun–planet and ring–planet meshes are modelled as rectangular waveforms with different contact ratios and mesh phasing. The operating conditions leading to parametric instability are analytically identified. Using the well-defined properties of planetary gear vibration modes, the boundaries separating stable and unstable conditions are obtained as simple expressions in terms of mesh parameters. These expressions allow one to suppress particular instabilities by adjusting the contact ratios and mesh phasing. Tooth separation from parametric instability is numerically simulated to show the strong impact of this non-linearity on the response.

1. INTRODUCTION

Mesh stiffness variation as the number of teeth in contact changes is a primary excitation of gear vibration and noise. This excitation exists even when the gears are perfectly machined and assembled. In analytical gear vibration models, it is represented by time-varying mesh stiffnesses that parametrically excite the system. This parametric excitation causes instability under certain operating conditions. The ensuing vibration creates noise, increases dynamic loads, and potentially damages the gear teeth and bearings [1].

Parametric instability in single-pair gears governed by a single-degree-of-freedom Mathieu equation has been extensively investigated [2–6]. For multi-stage gear systems, there are surprisingly few studies on parametric instabilities from multiple meshes. Tordion and Gauvin [7] and Benton and Seireg [8] analyzed the instabilities of two-stage gear systems with a mesh phasing between the two mesh stiffnesses. However, their instability conclusions are contradictory. This was recently clarified by Lin and Parker [9] using perturbation and numerical analyses. Lin and Parker also derived simple formulae that allow designers to suppress particular instabilities by properly selecting contact ratios and mesh phasing. For planetary gears (Figure 1), which have multiple time-varying mesh stiffnesses, no systematic study on their parametric instability has been found in the literature. August and Kasuba [10] and Velex and Flamand [11] numerically computed dynamic responses to mesh stiffness variations for planetary gears with three sequentially

0022-460X/02/010129 + 17 $35.00/0

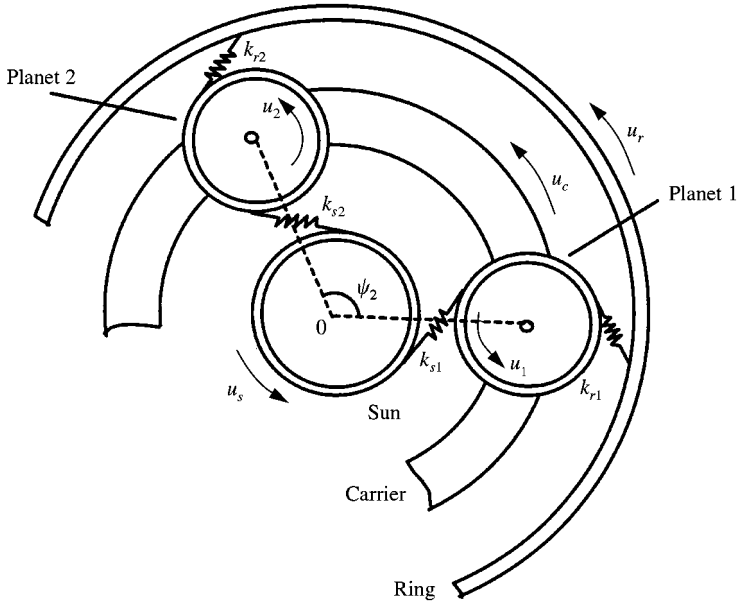

Figure 1. Rotational degree-of-freedom model of planetary gears.

phased planets. Their results showed the dramatic impact of mesh stiffness variation on dynamic response, tooth loads, and load sharing among planets. In addition, different contact ratios and phasing conditions that exist at the multiple meshes complicate the analytical examination of planetary gear parametric instability. How these factors affect instability conditions has not been investigated.

The objective of this study is to analyze parametric instability excited by multiple time-varying mesh stiffnesses in planetary gears. The torsional vibration model used here considers the different contact ratios and planet phasing among multiple meshes, which are critical design parameters in planetary gears. The well-defined modal properties of planetary gears [12, 13] are used to derive simple expressions for instability boundaries separating the stable and unstable regions. From these expressions, the effects of contact ratios and mesh phasing are analytically determined. These results provide insight into planetary gear designs that avoid parametric instability. In practice, planet mesh-phasing schemes are often applied to cancel or neutralize the resonant response at speeds where the mesh frequency is near a natural frequency [14–17]. In this same spirit, this study shows that particular parametric instabilities can be eliminated under certain phasing conditions that can be achieved by proper selection of design parameters. Tooth separation non-linearity induced by parametric instability is numerically simulated and shown to have great impact on the unstable system responses.

2. SYSTEM MODEL AND MODAL PROPERTIES

The planetary gear dynamic model used is based on the one developed by Lin and Parker [12]. Translational degrees of freedom in that model are eliminated, and only rotational motions of the gear bodies are considered (Figure 1). Rotational motions of the carrier, ring, sun, and planets are denoted by θ_h, $h = c, r, s, 1, \ldots, N$, where N indicates the number of

planets. The gear bodies are assumed rigid with moments of inertia I_c, I_r, I_s, I_p. The sun–planet and ring–planet tooth meshes are modelled as linear springs with time-varying stiffnesses $k_{sn}(t)$, $k_{rn}(t)$, $n = 1, \dots, N$. Damping and clearance non-linearity are not considered in the determination of instability boundaries, though they are added later in a numerical example for response calculation. The system's equations of motion are

$$\mathbf{M}\ddot{\mathbf{q}} + \mathbf{K}(t)\mathbf{q} = \mathbf{F}, \tag{1}$$

$$\mathbf{M} = \mathrm{diag}\lfloor I_c/r_c^2 + \Sigma m_p, I_r/r_r^2, I_s/r_s^2, I_p/r_p^2, \dots, I_p/r_p^2 \rfloor,$$

$$\mathbf{K}(t) = \begin{bmatrix} \Sigma(k_{sn} + k_{rn}) & -\Sigma k_{rn} & -\Sigma k_{sn} & k_{r1} - k_{s1} & \cdots & k_{rN} - k_{sN} \\ & \Sigma k_{rn} & 0 & -k_{r1} & \cdots & -k_{rN} \\ & & \Sigma k_{sn} & k_{s1} & \cdots & k_{sN} \\ & & & k_{r1} + k_{s1} & 0 \quad \cdots \quad 0 & \\ & & & & \ddots \quad \ddots \quad \vdots & \\ & & & & \ddots \quad 0 & \\ \text{symmetric} & & & & & k_{rN} + k_{sN} \end{bmatrix}, \tag{2}$$

$$\mathbf{q} = [u_c, u_r, u_s, u_1, \dots, u_N]^{\mathrm{T}}, \qquad \mathbf{F} = [T_c/r_c, T_r/r_r, T_s/r_s, 0, \dots, 0]^{\mathrm{T}},$$

where the summation index n ranges from 1 to N. $u_h = r_h\theta_h$, $h = c, r, s, 1, \dots, N$ are base radius deflections, and r_h is the base circle radius for the sun, ring, and planets and the radius of the circle passing through the planet centers for the carrier. T_c, T_r, T_s are external torques. Each mesh stiffness is represented by

$$k_{sn}(t) = k_{sp} + k_{1n}(t), \quad k_{rn}(t) = k_{rp} + k_{2n}(t), \qquad n = 1, \dots, N, \tag{3}$$

where k_{sp}, k_{rp} are mean values and k_{1n}, k_{2n} are time-varying components of the nth sun–planet and ring–planet meshes. Expansion of k_{1n}, k_{2n} in Fourier series yields

$$k_{1n}(t) = 2k_{vs}\sum_{l=1}^{\infty}(a_{sn}^{(l)}\sin l\Omega t + b_{sn}^{(l)}\cos l\Omega t), \qquad k_{2n}(t) = 2k_{vr}\sum_{l=1}^{\infty}(a_{rn}^{(l)}\sin l\Omega t + b_{rn}^{(l)}\cos l\Omega t). \tag{4}$$

For spur gears, rectangular waves are often used to approximate mesh stiffness alternating between d and $d + 1$ pairs of teeth in contact. Figure 2 shows the mesh stiffness variations k_{1n}, k_{2n} with peak-to-peak amplitudes $2k_{vs}$, $2k_{vr}$, contact ratios c_s, c_r, and phasing angles $\gamma_{sn}T$, $(\gamma_{sr} + \gamma_{rn})T$. The sun–planet and ring–planet meshes have the identical mesh frequency $\Omega = 2\pi/T$. The sun–planet mesh stiffnesses between planets differ only by a time translation (or phase), i.e. $k_{sn}(t) = k_{s1}(t - \gamma_{sn}T)$. Likewise, $k_{rn}(t) = k_{r1}(t - \gamma_{rn}T)$ for the ring–planet meshes. Mesh phasing between planets is determined by planet position angles ψ_n and the numbers of teeth z_s, z_r for the sun and ring [15]. $\gamma_{sn} = \psi_n z_s/(2\pi)$ denotes the mesh phasing between the first and nth sun–planet meshes ($\gamma_{s1} = 0$); $\gamma_{rn} = \psi_n z_r/(2\pi)$ is the mesh phasing between the first and nth ring–planet meshes ($\gamma_{r1} = 0$); γ_{sr} is the phasing between the sun–planet and ring–planet meshes for a given planet; it is the same for each planet. The

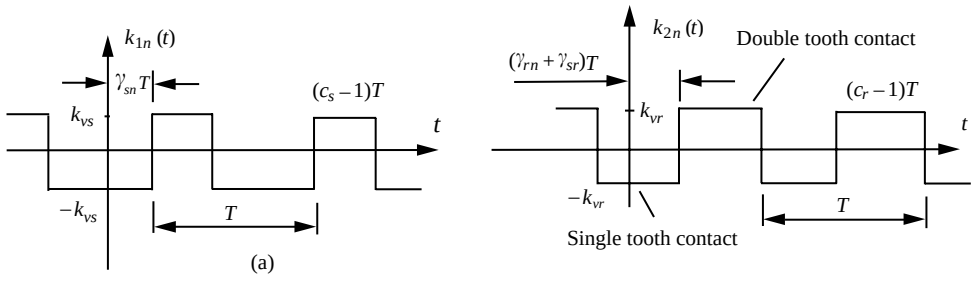

Figure 2. Modelling of mesh stiffness variations in the nth (a) sun–planet and (b) ring–planet meshes, c_s, c_r are contact ratios, and γ_{sn}, γ_{rn}, γ_{sr} are mesh phasing.

Fourier coefficients in equation (4) are

$$a_{sn}^{(l)} = -\frac{2}{l\pi}\sin\left[l\pi(c_s - 2\gamma_{sn})\right]\sin(l\pi c_s), \qquad a_{rn}^{(l)} = -\frac{2}{l\pi}\sin\left[l\pi(c_r - 2\gamma_{sr} - 2\gamma_{rn})\right]\sin(l\pi c_r),$$

$$b_{sn}^{(l)} = -\frac{2}{l\pi}\cos\left[l\pi(c_s - 2\gamma_{sn})\right]\sin(l\pi c_s), \qquad b_{rn}^{(l)} = -\frac{2}{l\pi}\cos\left[l\pi(c_r - 2\gamma_{sr} - 2\gamma_{rn})\right]\sin(l\pi c_r). \tag{5}$$

Mesh stiffnesses depend on many parameters including the number of teeth in contact, gear facewidth, material properties, profile modifications, and applied load [18]. Let $\varepsilon_1 = k_{vs}/k_{sp}$ and $\varepsilon_2 = k_{vr}/k_{rp}$ be the relative amplitudes of mesh stiffness variation. In the simplest approximation, mesh stiffnesses are assumed proportional to the number of tooth pairs in contact, that is, $k_{sp} = c_s\ k_{1t}$, $k_{rp} = c_r\ k_{2t}$ and $k_{vs} = k_{1t}/2$, $k_{vr} = k_{2t}/2$, where k_{1t}, k_{2t} are one-pair tooth bending stiffnesses of the sun–planet and ring–planet meshes. With this simplifying assumption, the nominal amplitudes of stiffness variations are $\varepsilon_1 = 1/(2c_s)$, $\varepsilon_2 = 1/(2c_r)$, and one obtains the explicit relation $\varepsilon_2 = \varepsilon_1 c_s/c_r$. In practice and in the analysis that follows, however, ε_1 and ε_2 are not constrained to these "nominal" values but vary independently of the contact ratios to account for the many factors influencing mesh stiffness variation amplitudes. For this modelling, we let $\varepsilon_1 = \varepsilon_2/g = \varepsilon$ where $g = O(1)$ (and $g = c_s/c_r$ under the simplifying assumption noted above). Substitution of equations (3) and (4) into equation (2) yields

$$\mathbf{K}(t) = \mathbf{K}_0 + 2\varepsilon\sum_{l=1}^{\infty}(\mathbf{K}_{v1}^{(l)}\sin l\Omega t + \mathbf{K}_{v2}^{(l)}\cos l\Omega t), \tag{6}$$

where the average stiffness matrix $\mathbf{K}_0$ has the same form as equation (2) with k_{sn}, k_{rn} substituted by k_{sp}, k_{rp}. The Fourier coefficient matrices are also in the form (2) with k_{sn}, k_{rn} substituted by $k_{sp}a_{sn}^{(l)}$, $gk_{rp}a_{rn}^{(l)}$ for $\mathbf{K}_{v1}^{(l)}$ and substituted by $k_{sp}b_{sn}^{(l)}$, $gk_{rp}b_{rn}^{(l)}$ for $\mathbf{K}_{v2}^{(l)}$.

For the time-invariant case, the eigenvalue problem associated with equation (1) is

$$\mathbf{K}_0\phi_i = \omega_i^2\mathbf{M}\phi_i, \tag{7}$$

where ω_i are the natural frequencies. The vibration modes ϕ_i are normalized as $\mathbf{\Phi}^{\mathrm{T}}\mathbf{M}\mathbf{\Phi} = \mathbf{I}$ with $\mathbf{\Phi} = [\phi_1, \ldots, \phi_L]$. The natural frequencies and vibration modes have unique

properties due to the cyclic symmetry of planetary gears [12, 13]. We specialize these properties for the case of a rotational vibration model with a fixed ring and $L = N + 2$ degrees of freedom. In this case, all vibration modes can be classified into one of three categories: (1) a rigid-body mode ($\omega_1 = 0$), (2) two modes with distinct natural frequencies (ω_2, ω_L), and (3) a group of degenerate modes with multiplicity $N - 1$ ($\omega_3 = \cdots = \omega_{N+1}$). In the distinct modes, including the rigid-body mode, all planets have identical motion,

$$u_n = u_1, \quad n = 1, 2, \ldots, N. \tag{8}$$

In the degenerate modes, the carrier, ring, and sun have no motion, and the planet rotations satisfy

$$u_n = [u_1 \sin(\psi_2 - \psi_n) + u_2 \sin\psi_n]/\sin\psi_2, \quad n = 1, 2, \ldots, N. \tag{9}$$

These well-defined properties are valid not only for equally spaced planets with position angles $\psi_n = 2\pi(n-1)/N$, but also for diametrically opposed planets with $\psi_{n+N/2} = \psi_n + \pi$ [13].

3. GENERAL EXPRESSIONS FOR INSTABILITY BOUNDARIES

Parametric instabilities occur when harmonics of the mesh frequency are close to particular combinations of the natural frequencies. We determine the operating conditions (that is, mesh frequency Ω and stiffness variation amplitude ε) that lead to instability when $l\Omega \approx \omega_p + \omega_g$ for integer l. The results are illustrated as stable and unstable regions in the (Ω, ε) parameter plane (Figure 3, for example). Primary ($l = 1$, $p = q$), secondary ($l = 2$, $p = q$), and combination ($l = 1$, $p \neq q$) instabilities are of most interest as higher order instabilities have much smaller instability regions and are unlikely to occur in practice. The rigid-body mode ($\omega_1 = 0$) is not excited under operating conditions and does not affect the instabilities of other modes. Only the two distinct modes and the group of degenerate modes are considered in what follows.

Applying the modal transformation $\mathbf{q} = \mathbf{\Phi z}$ to equation (1) and using equation (6), the free vibration equations become

$$\ddot{z}_i + \omega_i^2 z_i + 2\varepsilon \sum_{w=1}^{L} \sum_{l=1}^{\infty} (D_{iw}^{(l)} \sin l\Omega t + E_{iw}^{(l)} \cos l\Omega t) z_w = 0, \quad i = 2, \ldots, L, \tag{10}$$

where the matrices $\mathbf{D}^{(l)} = \mathbf{\Phi}^{\mathrm{T}} \mathbf{K}_{v1}^{(l)} \mathbf{\Phi}$ and $\mathbf{E}^{(l)} = \mathbf{\Phi}^{\mathrm{T}} \mathbf{K}_{v2}^{(l)} \Phi$. Using the method of multiple scales, the solution of equation (10) is expressed as

$$z_i = z_{i0}(t, \tau) + \varepsilon z_{i1}(t, \tau) + \cdots, \quad i = 2, \ldots, L, \tag{11}$$

where $\tau = \varepsilon t$ and $\mathrm{d}/\mathrm{d}t \to \partial/\partial t + \varepsilon \partial/\partial \tau$. Substitution of equation (11) into equation (10) yields

$$\frac{\partial^2 z_{i0}}{\partial t^2} + \omega_i^2 z_{i0} = 0, \quad i = 2, \ldots, L, \tag{12}$$

$$\frac{\partial^2 z_{i1}}{\partial t^2} + \omega_i^2 z_{i1} = -2 \frac{\partial^2 z_{i0}}{\partial t \, \partial \tau} - 2 \sum_{w=1}^{L} \sum_{l=1}^{\infty} [D_{iw}^{(l)} \sin l\Omega t + E_{iw}^{(l)} \cos l\Omega t] z_{w1}, \quad i = 2, \ldots, L. \tag{13}$$

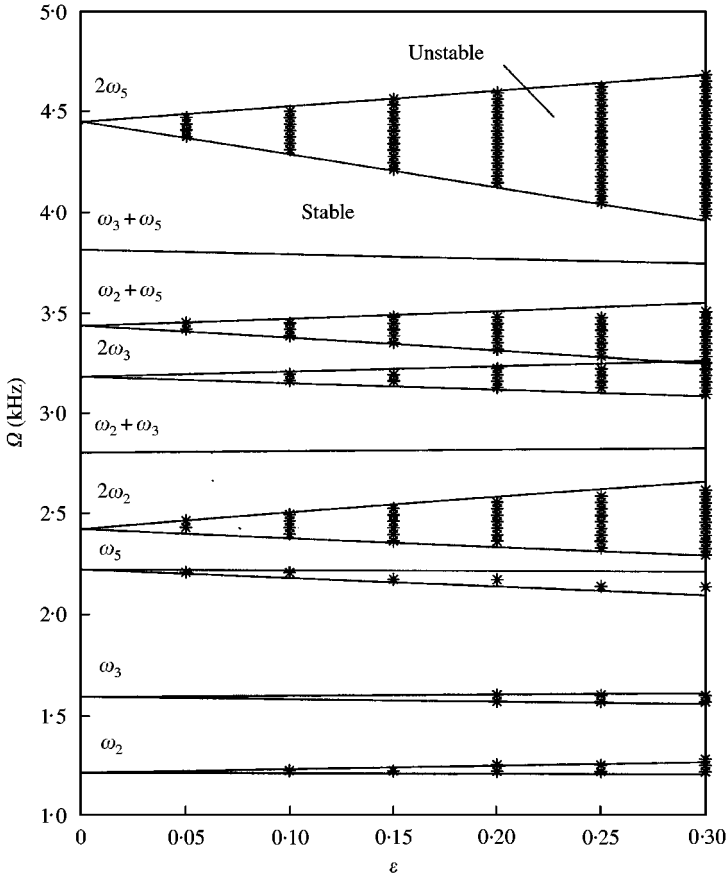

Figure 3. Instability regions for the three-planet system in Table 1 and in-phase meshes $\gamma_{sn} = \gamma_{rn} = 0$, $\gamma_{sr} = \frac{1}{2}$. $c_s = 1{\cdot}4$, $c_r = 1{\cdot}6$, $\varepsilon = \varepsilon_1 = \varepsilon_2$ ($g = 1$). —, Analytical solution; ***, numerical solution.

The general solutions of equation (12) are

$$z_{i0} = A_i(\tau)\mathrm{e}^{\mathrm{j}\omega_i t} + \mathrm{cc}, \quad i = 2, \ldots, L, \tag{14}$$

where cc represents the complex conjugate of preceding terms. Insertion of equation (14) into equation (13) yields

$$\frac{\partial^2 z_{i1}}{\partial t^2} + \omega_i^2 z_{i1} = -2\mathrm{j}\omega_i \mathrm{e}^{\mathrm{j}\omega_i t}\frac{\partial A_i}{\partial \tau} - \sum_{w=1}^{L}\sum_{l=1}^{\infty} A_w\left[(D_{iw}^{(l)} - \mathrm{j}E_{iw}^{(l)})\mathrm{e}^{\mathrm{j}(\omega_i + l\Omega)t} + (D_{iw}^{(l)} + \mathrm{j}E_{iw}^{(l)})\mathrm{e}^{\mathrm{j}(\omega_i - l\Omega)t}\right] + \mathrm{cc}, \quad i = 2, \ldots, L. \tag{15}$$

The parametric instability when $l\Omega \approx \omega_p + \omega_q$ is considered. Let $l\Omega = \omega_p + \omega_q + \varepsilon\sigma$, where σ is a detuning parameter to be determined. When ω_p and ω_q are both distinct, the

instability boundaries are as follows [9]:

$$\text{Single mode instability: } \Omega = \frac{2\omega_p}{l} \pm \frac{\varepsilon}{l\omega_p}\sqrt{\Lambda_{pp}^{(l)}}; \tag{16}$$

$$\text{Combination instability: } \Omega = \frac{\omega_p + \omega_q}{l} \pm \frac{\varepsilon}{l}\sqrt{\Lambda_{pq}^{(l)}/(\omega_p\omega_q)}, \tag{17}$$

where $\Lambda_{pq}^{(l)} = (D_{pq}^{(l)})^2 + (E_{pq}^{(l)})^2$.

When ω_p or ω_q is degenerate, the complexity of instability boundary solutions depends on the multiplicity of the degenerate natural frequencies. We first study the case with multiplicity two for three-planet systems, say $\omega_p = \omega_q$. For the single-mode instability $l\Omega = 2\omega_p + \varepsilon\sigma$, vanishing of the terms in equation (15) leading to unbounded response requires

$$2\mathrm{j}\omega_p \partial A_p/\partial\tau + [(D_{pp}^{(l)} + \mathrm{j}E_{pp}^{(l)})\bar{A}_p + (D_{pq}^{(l)} + \mathrm{j}E_{pq}^{(l)})\bar{A}_q]\mathrm{e}^{\mathrm{j}\sigma\tau} = 0, \tag{18}$$

$$2\mathrm{j}\omega_q \partial A_q/\partial\tau + [(D_{qp}^{(l)} + \mathrm{j}E_{qp}^{(l)})\bar{A}_p + (D_{qq}^{(l)} + \mathrm{j}E_{qq}^{(l)})\bar{A}_q]\mathrm{e}^{\mathrm{j}\sigma\tau} = 0. \tag{19}$$

The non-trivial solutions of equations (18) and (19) have the form

$$A_p = (R_p + \mathrm{j}I_p)\mathrm{e}^{\mathrm{j}\sigma\tau/2}, \qquad A_q = (R_q + \mathrm{j}I_q)\mathrm{e}^{\mathrm{j}\sigma\tau/2}, \tag{20}$$

where R_p, R_q, I_p, I_q are real. With these solutions, equations (18) and (19) yield

$$2\omega_p \frac{\partial}{\partial\tau}\begin{bmatrix} I_p \\ I_q \\ R_p \\ R_q \end{bmatrix} = \begin{bmatrix} E_{pp}^{(l)} & E_{pq}^{(l)} & D_{pp}^{(l)} - \sigma\omega_p & D_{pq}^{(l)} \\ E_{qp}^{(l)} & E_{qq}^{(l)} & D_{qp}^{(l)} & D_{qq}^{(l)} - \sigma\omega_q \\ D_{pp}^{(l)} + \sigma\omega_p & D_{pq}^{(l)} & -E_{pp}^{(l)} & -E_{pq}^{(l)} \\ D_{qp}^{(l)} & D_{qq}^{(l)} + \sigma\omega_q & -E_{qp}^{(l)} & -E_{qq}^{(l)} \end{bmatrix}\begin{bmatrix} I_p \\ I_q \\ R_p \\ R_q \end{bmatrix}. \tag{21}$$

For bounded solutions, the eigenvalues of the coefficient matrix have non-positive real parts, which requires

$$\sigma \geqslant \sqrt{\Gamma^{(l)}}/\omega_p, \qquad \Gamma^{(l)} = D_{pq}^{(l)}D_{qp}^{(l)} + E_{pq}^{(l)}E_{qp}^{(l)} + \tfrac{1}{2}[(D_{pp}^{(l)})^2 + (D_{qq}^{(l)})^2 + (E_{pp}^{(l)})^2 + (E_{qq}^{(l)})^2]. \tag{22}$$

Thus, the single-mode instability boundaries for $\omega_p = \omega_q$ are

$$\Omega = \frac{2\omega_p}{l} \pm \frac{\varepsilon}{l\omega_p}\sqrt{\Gamma^{(l)}}. \tag{23}$$

Now consider the combination instability $l\Omega = \omega_p + \omega_r + \varepsilon\sigma$, where $\omega_p = \omega_q$ are degenerate but ω_r is distinct. Vanishing of the terms in equation (15) leading to unbounded response requires

$$2\mathrm{j}\omega_r \partial A_r/\partial\tau + (D_{rp}^{(l)} + \mathrm{j}E_{rp}^{(l)})\bar{A}_p + (D_{rq}^{(l)} + \mathrm{j}E_{rq}^{(l)})\bar{A}_q]\mathrm{e}^{\mathrm{j}\sigma\tau} = 0, \tag{24}$$

$$2\mathrm{j}\omega_p \partial A_p/\partial\tau + (D_{pr}^{(l)} + \mathrm{j}E_{pr}^{(l)})\bar{A}_r\mathrm{e}^{\mathrm{j}\sigma\tau} = 0, \tag{25}$$

$$2\mathrm{j}\omega_q \partial A_q/\partial\tau + (D_{qr}^{(l)} + \mathrm{j}E_{qr}^{(l)})\bar{A}_r\mathrm{e}^{\mathrm{j}\sigma\tau} = 0. \tag{26}$$

With the solutions (20) and $A_r = (R_r + \mathrm{j}I_r)\mathrm{e}^{\mathrm{j}\sigma\tau/2}$, equations (24)–(26) give

$$2\frac{\partial}{\partial\tau}\begin{bmatrix} I_r \\ I_p \\ I_q \\ R_r \\ R_p \\ R_q \end{bmatrix} = \begin{bmatrix} 0 & E_{rp}^{(l)}/\omega_r & E_{rq}^{(l)}/\omega_r & -\sigma & D_{rp}^{(l)}/\omega_r & D_{rq}^{(l)}/\omega_r \\ E_{pr}^{(l)}/\omega_p & 0 & 0 & D_{pr}^{(l)}/\omega_p & -\sigma & 0 \\ E_{qr}^{(l)}/\omega_q & 0 & 0 & D_{qr}^{(l)}/\omega_q & 0 & -\sigma \\ \sigma & D_{rp}^{(l)}/\omega_r & D_{rq}^{(l)}/\omega_r & 0 & E_{rp}^{(l)}/\omega_r & -E_{rq}^{(l)}/\omega_r \\ D_{pr}^{(l)}/\omega_{/p} & \sigma & 0 & -E_{pr}^{(l)}/\omega_p & 0 & 0 \\ D_{qr}^{(l)}/\omega_q & 0 & \sigma & -E_{qr}^{(l)}/\omega_q & 0 & 0 \end{bmatrix} \begin{bmatrix} I_r \\ I_p \\ I_q \\ R_r \\ R_p \\ R_q \end{bmatrix}. \quad (27)$$

Requiring the eigenvalues of the coefficient matrix to have non-positive real parts gives the instability boundaries

$$\Omega = \frac{\omega_p + \omega_r}{l} \pm \frac{\varepsilon}{l}\left[(D_{pr}^{(l)}D_{rp}^{(l)} + D_{qr}^{(l)}D_{rq}^{(l)} + E_{pr}^{(l)}E_{rp}^{(l)} + E_{qr}^{(l)}E_{rq}^{(l)})/(\omega_p\omega_r)\right]^{1/2}. \quad (28)$$

When the degenerate natural frequencies $\omega_3 = \cdots = \omega_{m+2}$ have multiplicity $m > 2$, vanishing of the terms in equation (15) leading to an unbounded response for $l\Omega = 2\omega_p + \varepsilon\sigma$ yields m coupled equations

$$2\mathrm{j}\omega_p\partial A_p/\partial\tau + \sum_{q=3}^{m+2}(D_{pq}^{(l)} + \mathrm{j}E_{pq}^{(l)})\bar{A}_g\mathrm{e}^{\mathrm{j}\sigma\tau} = 0, \quad p = 3, \ldots, m+2. \quad (29)$$

Similar to equation (21), a $2m \times 2m$ coefficient matrix is obtained from equation (29),

$$\begin{bmatrix} \mathbf{E}_{sub}^{(l)} & \mathbf{D}_{sub}^{(l)} - (\sigma\omega_3)\mathbf{I}_{m\times m} \\ \mathbf{D}_{sub}^{(l)} + (\sigma\omega_3)\mathbf{I}_{m\times m} & -\mathbf{E}_{sub}^{(l)} \end{bmatrix}, \quad (30)$$

where $\mathbf{D}_{sub}^{(l)}$, $\mathbf{E}_{sub}^{(l)}$ are $m \times m$ submatrices of $\mathbf{D}^{(l)}$, $\mathbf{E}^{(l)}$ including rows and columns $3, \ldots, m+2$. The σ for bounded solutions is obtained by requiring the real parts of the eigenvalues of this coefficient matrix to be non-positive. Generally, no closed-form solution can be derived for these single-mode instabilities, but numerical evaluation can determine σ and the instability boundaries unless $\mathbf{D}_{sub}^{(l)}$, $\mathbf{E}_{sub}^{(l)}$ have special features (e.g., diagonal matrices) as discussed later. More is possible for combination instabilities. For combination instability of distinct ω_r and degenerate $\omega_3 = \cdots = \omega_{m+2}$ of any multiplicity m, the same procedures as led to equation (28) yields instability boundaries

$$\Omega = \frac{\omega_3 + \omega_r}{l} \pm \frac{\varepsilon}{l}\sum_{q=3}^{m+3}\sqrt{(D_{qr}^{(l)}D_{rq}^{(l)} + E_{qr}^{(l)}E_{rq}^{(l)})/(\omega_r\omega_3)}. \quad (31)$$

All results so far apply for a general system (10) with degenerate natural frequencies. These results reduce to simple forms when specialized to planetary gears.

4. PLANETARY GEAR PARAMETRIC INSTABILITY

The planetary gears' well-defined modal properties are now used to simplify the above instability conditions to compact expressions suitable for use in applications. Expansion of

$\mathbf{D}^{(l)}$, $\mathbf{E}^{(l)}$ in equation (10) gives

$$D_{pq}^{(l)} = \phi_p^{\mathrm{T}} \mathbf{K}_{v1}^{(l)} \phi_q = k_{sp} \sum_{n=1}^{N} a_{sn}^{(l)} \delta_{sn}^{(p)} \delta_{sn}^{(q)} + k_{rp} g \sum_{n=1}^{N} a_{rn}^{(l)} \delta_{rn}^{(p)} \delta_{rn}^{(q)},$$

$$E_{pq}^{(l)} = \phi_p^{\mathrm{T}} \mathbf{K}_{v2}^{(l)} \phi_q = k_{sp} \sum_{n=1}^{N} b_{sn}^{(l)} \delta_{sn}^{(p)} \delta_{sn}^{(q)} + k_{rp} g \sum_{n=1}^{N} b_{rn}^{(l)} \delta_{rn}^{(p)} \delta_{rn}^{(q)}, \tag{32}$$

where $\delta_{sn}^{(p)} = u_s - u_c + u_n$ is the deformation of the nth sun–planet mesh in mode ϕ_p and $\delta_{rn}^{(p)} = -u_c - u_n$ is the deformation of the nth ring–planet mesh. For different spacing and phasing of planets, matrices $\mathbf{D}^{(l)}$, $\mathbf{E}^{(l)}$ have special features that simplify the instability conditions. Note that the following analysis considers mesh stiffness of any waveform as represented by the Fourier coefficients a, b in equation (32). As the most appropriate analytical idealization for spur gears, rectangular waveforms (5) are used to get simplified expressions and investigate the effects of contact ratio and phasing.

4.1. EQUALLY SPACED PLANETS

For equally spaced planets ($\psi_n = 2\pi(n-1)/N$), the vibration modes have structured properties (8) and (9). In this case, $(z_s + z_r)/N =$ integer and the planet meshes have phasing $\gamma_{sn} = (n-1)z_s/N$ and $\gamma_{rn} = -(n-1)z_r/N$, $n = 1, \ldots, N$. The two possible phasing conditions are examined below.

4.1.1. *In-phase planet meshes*

Consider the case when all the sun–planet meshes are in-phase ($\gamma_{sn} = 0, n = 1, \ldots, N$) and all the ring–planet meshes are in-phase ($\gamma_{rn} = 0,\ n = 1, \ldots, N$). This design is typical when optimizing load shared among planets and results when z_s and z_r are each integer multiples of N. There is, however, a constant phasing γ_{sr} between the sun–planet and ring–planet meshes for each planet. The Fourier coefficients $a_{sn}^{(l)}$, $a_{rn}^{(l)}$, $b_{sn}^{(l)}$, $b_{rn}^{(l)}$ in (4) and (32) are independent of the plant index n for in-phase planet meshes.

For a distinct natural frequency ω_p, vibration mode property (8) leads to $\delta_{sn}^{(p)} = \delta_{s1}^{(p)}$, $\delta_{rn}^{(p)} = \delta_{r1}^{(p)}$ for any planet n. Using rectangular form (5) and (32) in equation (16), the primary instability boundaries are governed by

$$\Lambda_{pp}^{(1)} = \left(\frac{2N}{\pi}\right)^2 [(\delta_{s1}^{(p)})^4 (k_{sp} \sin \pi c_s)^2 + (\delta_{r1}^{(p)})^4 (k_{rp} g \sin \pi c_r)^2$$

$$+ 2k_{sp} k_{rp} g (\delta_{s1}^{(p)} \delta_{r1}^{(p)})^2 \sin(\pi c_s) \sin(\pi c_r) \cos \pi (c_s - c_r + 2\gamma_{sr})]. \tag{33}$$

Obviously, $\Lambda_{pp}^{(1)} = 0$ when c_s, c_r are integers and all instabilities vanish. If c_s, $c_r \neq$ integer, a second choice to reduce the instability regions is to make the third term in equation (33) negative by adjusting c_s, c_r, and γ_{sr}. The combination instability boundaries for two distinct modes can be obtained from equation (17).

For the degenerate natural frequencies $\omega_3 = \cdots = \omega_{N+1}$, vibration mode property (9) results in

$$\sum_{n=1}^{N} \delta_{sn}^{(p)} \delta_{sn}^{(q)} = \sum_{n=1}^{N} \delta_{rn}^{(p)} \delta_{rn}^{(q)} = 0, \quad \sum_{n=1}^{N} (\delta_{sn}^{(p)})^2 = \sum_{n=1}^{N} (\delta_{rn}^{(p)})^2 = \Delta, \qquad p, q = 3, \ldots, N+1, \quad p \neq q, \tag{34}$$

where the following identities are used to derive equation (34):

$$\sum_{n=1}^{N} \cos \frac{2\pi(n-1)Z}{N} = \sum_{n=1}^{N} \sin \frac{2\pi(n-1)Z}{N} = 0, \quad \text{for non-integer } Z/N. \tag{35}$$

Use of equation (34) in equation (32) gives

$$D_{pq}^{(l)} = E_{pq}^{(l)} = 0, \quad D_{pp}^{(l)} = (k_{sp} a_{s1}^{(l)} + k_{rp} g a_{r1}^{(l)})\Delta, \quad E_{pp}^{(p)} = (k_{sp} b_{s1}^{(l)} + k_{rp} g b_{r1}^{(l)})\Delta, \qquad p, q = 3, \ldots, N+1. \tag{36}$$

For the simple form of $D_{pq}^{(l)}$, $E_{pq}^{(l)}$ in equation (36), the eigenvalues of equation (30) can be expressed in closed form for any multiplicity $m = N - 1$. In this case, the single-mode instability boundaries are the same as equation (23) with $\Gamma^{(l)} = (D_{pp}^{(l)})^2 + (E_{pp}^{(l)})^2$. For the rectangular waveforms (5),

$$\Gamma^{(l)} = \left(\frac{2\Delta}{l\pi}\right)^2 [(k_{sp} \sin l\pi c_s)^2 + (k_{rp} g \sin l\pi c_r)^2 + 2k_{sp} k_{rp} g \sin(l\pi c_r) \sin(l\pi c_r) \cos l\pi(c_s - c_r + 2\gamma_{sr})]. \tag{37}$$

Equation (37) applies for any number of planets N.

For the combination instability of degenerate $\omega_3 = \cdots = \omega_{N+1}$ and distinct ω_r, use of properties (8) and (9) in equation (32) yields

$$D_{pr}^{(l)} = \sum_{n=1}^{N} \left\{ C_1 \cos\left[\frac{2\pi(n-1)(lz_s+1)}{N} + \beta_1\right] + C_2 \cos\left[\frac{2\pi(n-1)(lz_s-1)}{N} + \beta_2\right] + C_3 \cos\left[\frac{2\pi(n-1)(lz_r+1)}{N} + \beta_3\right] + C_4 \cos\left[\frac{2\pi(n-1)(lz_r-1)}{N} + \beta_4\right]\right\}, \quad p = 3, \ldots, N+1, \tag{38}$$

where C_i and β_i are constants independent of n. For in-phase planet meshes (z_s/N, z_r/N are integers) and $l = 1$, equation (35) guarantees $D_{pr}^{(l)} = 0$ and similarly $E_{pr}^{(l)} = 0$. It follows from equation (31) that the combination instabilities ($l = 1$) of a distinct mode and a degenerate mode *always* vanish for any N when the planet meshes are in-phase. A more general condition for vanishing of these combination instabilities is that each of $(lz_s \pm 1)/N$, $(lz_r \pm 1)/N \neq$ integer.

As an example, Figure 3 shows the instability boundaries for a planetary gear with three equally spaced planets. The parameters and nominal natural frequencies are given in

TABLE 1

Parameters and natural frequencies of an example planetary gear with fixed ring and three planets

Inertias (kg)	$I_c/r_c^2 = 6$, $I_s/r_s^2 = 2{\cdot}5$, $I_p/r_p^2 = 2$
Planet mass (kg)	$m_p = 4$
Mesh stiffness (N/m)	$k_{sp} = k_{rp} = 10^8$
Natural frequencies (kHz)	$\omega_1 = 0$, $\omega_2 = 1{\cdot}212$, $\omega_3 = \omega_4 = 1{\cdot}592$, $\omega_5 = 2{\cdot}196$

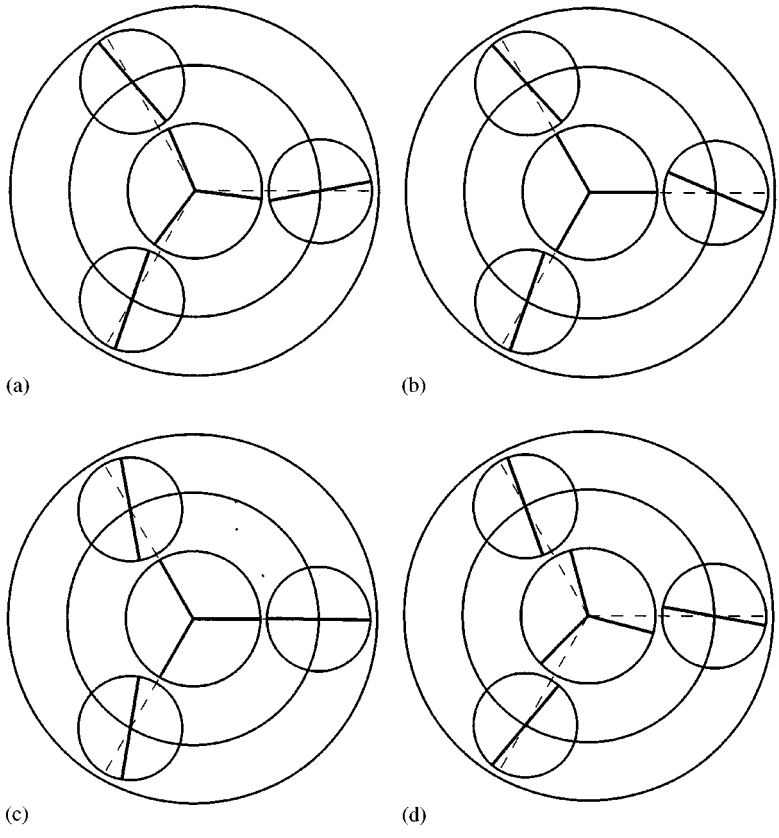

Figure 4. Mode shapes of the system in Table 1. The motion of the carrier is not shown. (a) $\omega_2 = 1212$ Hz, (b) $\omega_3 = 1592$ Hz, (c) $\omega_4 = 1592$ Hz, (d) $\omega_5 = 2196$ Hz.

Table 1 and the vibration modes are shown in Figure 4. The mesh phasing $\gamma_{sn} = \gamma_{rn} = 0$, $\gamma_{sr} = \frac{1}{2}$ and the contact ratios $c_s = 1{\cdot}4$, $c_r = 1{\cdot}6$. We specify $\varepsilon_1 = \varepsilon_2 = \varepsilon$ (i.e., $g = 1$). The slight downward drift in the instability regions results from natural frequency changes as ε varies, which occur because the average mesh stiffnesses depend on k_{vs} and k_{vr} (the central line between the peak-to-peak mesh stiffnesses in Figure 2 are held constant). The analytical solutions (solid lines) from equations (16), (17), (23), and (28) agree well with the numerical solutions using the Floquet theory and numerical integration. Note that the combination instabilities at $\omega_2 + \omega_3$, $\omega_3 + \omega_5$ vanish because they involve the distinct (ω_2, ω_5) and degenerate ($\omega_3 = \omega_4$) natural frequencies. Figure 5(a) shows the primary instability regions for different contact ratios c_s, c_r; the stiffness variation amplitude $\varepsilon = 0{\cdot}3$ and phasing

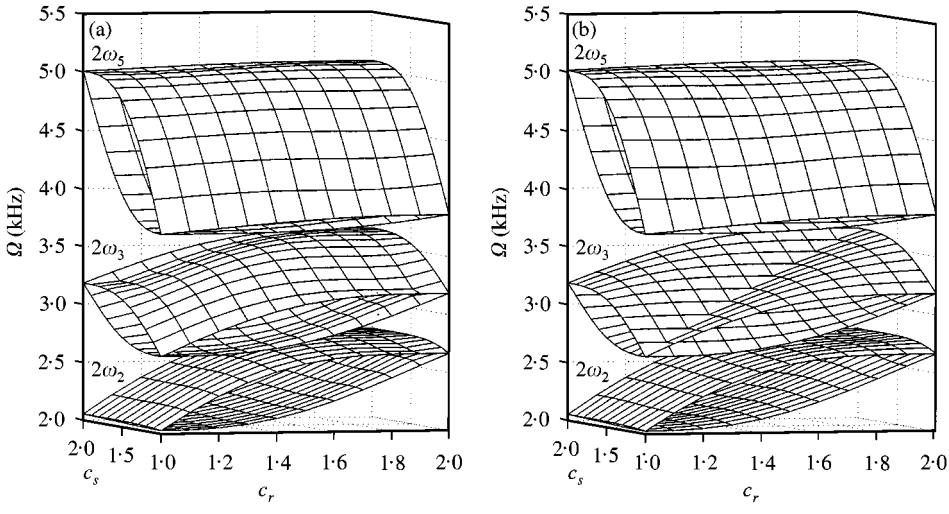

Figure 5. Instability regions of the system in Table 1 for different contact ratios. $\varepsilon = \varepsilon_1 = \varepsilon_2 = 0{\cdot}3$ ($g = 1$). The planets are equally spaced with in-phase meshes ($\gamma_{sn} = \gamma_{rn} = 0$). (a) $\gamma_{sr} = 0$, (b) $\gamma_{sr} = \frac{1}{2}$.

$\gamma_{sr} = 0$. All instabilities vanish when the contact ratios are integers. The size of the $2\omega_2$ instability region is primarily affected by c_r while insensitive to changes in c_s. This is because the dominant deformation of mode ϕ_2 occurs in the ring–planet meshes (Figure 4). The $2\omega_5$ instability region is mostly affected by c_s because most deformation occurs in the sun–planet meshes for this mode. The primary instability of the degenerate modes at $2\omega_3 = 2\omega_4$ is influenced by both c_s and c_r. The primary instability regions are maximized for $c_s = c_r = 1{\cdot}5$, which is expected from equations (33) and (37). The relative phasing γ_{sr} between the sun–planet and ring–planet meshes can have a major impact. When the phasing $\gamma_{sr} = \frac{1}{2}$ (Figure 5(b)), the $2\omega_3 = 2\omega_4$ instability vanishes for any $c_s = c_r$ because $\Gamma^{(l)} = 0$ in equation (37) in this case.

4.1.2. *Sequentially phased planet meshes*

Here we consider equally spaced planet systems where the sun–planet and ring–planet meshes are sequentially phased with $\gamma_{sn} = (n-1)z_s/N$ and $\gamma_{rn} = -(n-1)z_r/N$. This case corresponds to z_s/N, $z_r/N \neq$ integer but $(z_s + z_r)/N =$ integer. A constant phasing γ_{sr} exists between the sun–planet and ring–planet meshes for each planet. Using equation (35) and the sequential phasing, the Fourier coefficients in equation (32) satisfy

$$\sum_{n=1}^{N} a_{sn}^{(l)} = \sum_{n=1}^{N} a_{rn}^{(l)} = \sum_{n=1}^{N} b_{sn}^{(l)} = \sum_{n=1}^{N} b_{rn}^{(l)} = 0 \tag{39}$$

where lz_s/N, lz_r/N are non-integer. Equation (39) applies for any mesh stiffness variation waveform.

For distinct natural frequencies ω_p, using $\delta_{sn} = \delta_{s1}$ and equation (39) in equation (32) yields $D_{pp}^{(l)} = E_{pp}^{(l)} = 0$. It follows from equation (16) that the primary instabilities ($l = 1$) of distinct modes *always* vanish when the planets are sequentially phased. Physically, it means that these instabilities are not excited because the resultant modal excitations from the sun–planet and ring–planet meshes each are zero. The secondary instabilities ($l = 2$) of

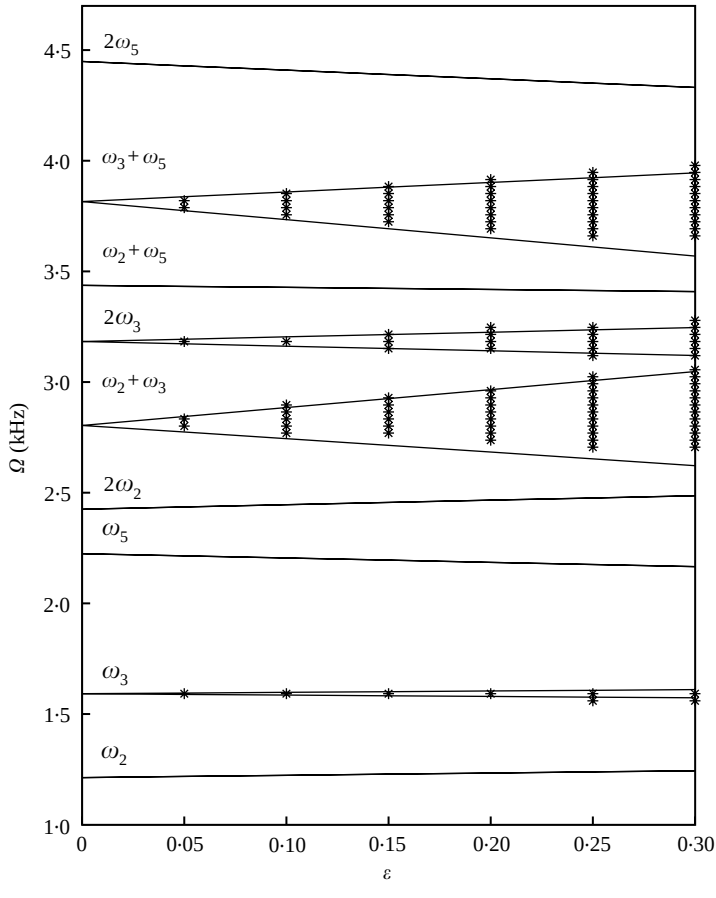

Figure 6. Instability regions for the system in Table 1 and sequentially phased planet meshes with $\gamma_{sn} = [0, \frac{1}{3}, \frac{2}{3}]$, $\gamma_{rn} = [0, -\frac{2}{3}, -\frac{1}{3}]$. $c_s = 1{\cdot}4$, $c_r = 1{\cdot}6$, $\varepsilon = \varepsilon_1 = \varepsilon_2$ $(g = 1)$, $\gamma_{sr} = \frac{1}{2}$. —, Analytical solution; ***, numerical solution.

distinct modes also vanish when $2z_s/N$, $2z_r/N$ are non-integers. Similarly, for the combination instability ($l = 1$) of distinct ω_p and ω_q, $D_{pp}^{(1)} = E_{pp}^{(1)} = 0$ in equation (17). Thus, combination instabilities of two distinct modes *always* vanish in this case.

For instabilities involving the degenerate modes, it is difficult to obtain simple expressions for the instability boundaries; their instability conditions can be calculated from equations (23), (30), and (31). A special case is the combination instability ($l = 1$) of degenerate $\omega_3 = \cdots = \omega_{N+1}$ and distinct ω_r when both $(z_s \pm 1)/N$, $(z_r \pm 1)/N$ are non-integers. In this case, $D_{pr}^{(1)} = E_{pr}^{(1)} = 0$, $p = 3, \ldots, N + 1$ because of equations (35) and (38), and the combination instabilities of distinct and degenerate modes vanish.

Figure 6 shows the instability boundaries for the same system as in Figure 3, except that the three planets are sequentially phased with $\gamma_{sn} = [0, \frac{1}{3}, \frac{2}{3}]$, $\gamma_{rn} = [0, -\frac{2}{3}, -\frac{1}{3}]$. Note that the primary, secondary, and combination instability regions vanish for the distinct natural frequencies ω_2, ω_5; only instabilities involving the degenerate modes $\omega_3 = \omega_4$ exist.

The above analyses show that contact ratios and mesh phasing significantly affect the operating condition instability regions. In practice, particular instabilities can be minimized by proper selection of contact ratios and mesh phasing, which are adjusted by center distance, diametral pitch, pressure angle, tooth addendum, numbers of teeth, and other

TABLE 2

Instability boundary solutions when the planets are equally spaced (satisfying $(z_s + z_r)/N = integer$)

Planet mesh phasing	Single-mode instabilities		Combination instabilities	
	Distinct mode	Degenerate mode	Distinct + distinct mode	Degenerate + distinct mode
In-phase $\frac{z_s}{N}, \frac{z_r}{N} = \text{integer}$	From equation (16)	From equations (22), (23), (30)	From equation (17)	Always vanish
Sequentially phased $\frac{z_s}{N}, \frac{z_r}{N} \neq \text{integer}$	Primary always vanish; secondary from equation (16) and vanish if $2z_s/N, 2z_r/N \neq$ integer	From equations (22), (23), (30)	Always vanish	From equation (31) and vanish if $(z_s \pm 1)/N$, $(z_r \pm 1)/N \neq$ integer

parameters. The foregoing results for equally spaced planets and any mesh stiffness waveform (not just rectangular) are summarized in Table 2.

4.2. UNEQUALLY SPACED PLANETS

When the planets are arbitrarily spaced, the structured modal properties do not exist and the general expressions for instability boundaries cannot be further simplified. For the practically important case of diametrically opposed planets, however, the vibration modes retain the well-defined properties (8) and (9). For the sun–planet meshes, each of the $N/2$ pairs of diametrically opposed planets are in-phase ($\gamma_{s(n+N/2)} = \gamma_{sn}$) for even z_s and counter-phased ($\gamma_{s(n+N/2)} = \gamma_{sn} + 1/2$) for odd z_s. An analogous rule applies for the ring–planet mesh phasing. Note that adjacent planets have arbitrary mesh phasing defined by their circumferential position, $\gamma_{sn} = \psi_n z_s/(2\pi)$, $\gamma_{rn} = -\psi_n z_r/(2\pi)$, $n = 1, \ldots, N/2$.

When the sun–planet and ring–planet meshes are both counter-phased (odd z_s, z_r), equation (39) holds for odd l because $a_{sn}^{(l)} = -a_{s(n+N/2)}^{(l)}$ and similar relations for $a_{rn}^{(l)}, b_{sn}^{(l)}, b_{rn}^{(l)}$. Recalling the modal property (8), $D_{pq}^{(l)} = E_{pq}^{(l)} = 0$ for distinct ω_p, ω_q and odd l. From equations (16) and (17), primary and combination ($l = 1$) instabilities of distinct modes *always* vanish in the counter-phased case. Physically, these instabilities are eliminated because the modal excitations from each pair of diametrically opposed planets always cancel each other. The instability regions involving degenerate modes are obtained from numerical evaluation of the eigenvalues of equation (30).

When pairs of opposing sun–planet or ring–planet meshes are in-phase (even z_s or even z_r), no simple expression for instabilities regions is available; numerical solutions are obtained from equations (16), (17), (30), and (31).

5. DYNAMIC RESPONSE AND CONTACT LOSS

When planetary gears operate inside an instability region, damping and non-linearities from friction, tooth separation, etc., bound the unstable linear model motion. Figure 7(a) shows the r.m.s. steady state planet response amplitude versus mesh frequency for the same

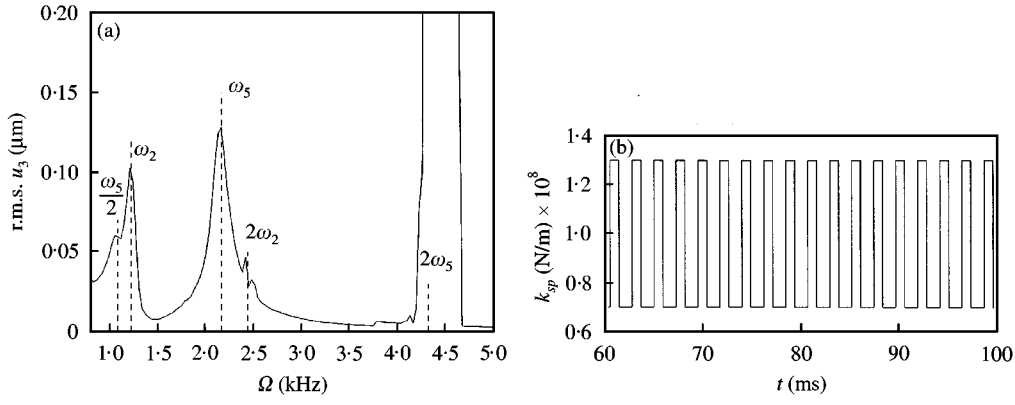

Figure 7. (a) Steady state r.m.s. of dynamic planet rotation versus mesh frequency Ω when tooth separation is not considered. The parameters are as in Figure 3 with $\varepsilon = 0{\cdot}3$. (b) The sun–planet mesh stiffness is pre-specified as shown.

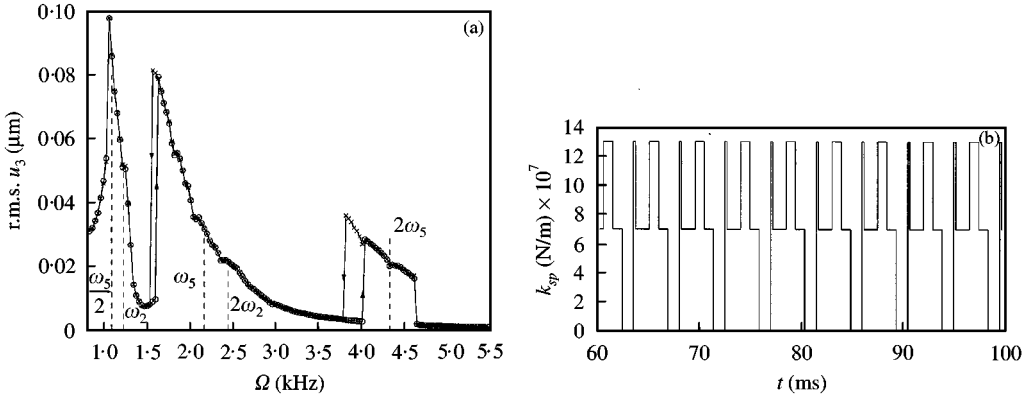

Figure 8. (a) Steady state r.m.s. of dynamic planet rotation versus mesh frequency Ω when tooth separation is considered. The parameters are as in Figure 3 with $\varepsilon = 0{\cdot}3$. Circles (○) indicate increasing speed Ω and crosses (×) indicate decreasing Ω. (b) Sun–planet tooth separation ($k_{sp} = 0$) occurs for $\Omega = 4{\cdot}5$ kHz $\approx 2\,\omega_5$.

system as in Figure 3 and the stiffness variation $\varepsilon = 0{\cdot}3$. Rayleigh damping $\mathbf{C} = (0{\cdot}07) * \mathbf{M} + (0{\cdot}07) * \mathbf{K}$ is added to system (1) and the force vector is $\mathbf{F} = [-2000\ 1000\ 0\ 0\ 0]^{\mathrm{T}}$ N. The solutions are obtained from numerical integration of equation (10) using mesh stiffnesses in rectangular waveforms (Figure 7(b)). The instabilities near $\omega_3 = \omega_4$, $2\omega_3 = 2\omega_4$, and $\omega_2 + \omega_5$ grow to instability very slowly so that their parametric instabilities are not apparent in Figure 7(a) (and Figure 8(a)). The instability excited by the primary instability $2\omega_5$ grows extremely large because tooth separation (that is, vanishing mesh stiffness) is *not* considered; the mesh stiffnesses are pre-specified functions of time (Figure 7(b)). In practice, tooth separation (clearance non-linearity) occurs for large dynamic responses and its effects are dramatic. Figure 8(a) shows the response for the same system as in Figure 7(a) but tooth separations are modelled. The mesh stiffness k_{sn} or k_{rn} is set to zero if the corresponding tooth deformation $\delta_{sn} < 0$ or $\delta_{rn} < 0$ at any step of the integration. The response amplitude of the $2\omega_5$ primary instability is *significantly* reduced from that in Figure 7(a). Moreover, a softening jump phenomenon occurs. Sun–planet tooth

separation ($k_{sp} = 0$) is apparent in Figure 8(b) for a mesh frequency in the primary instability region of $2\omega_5$. The interactions of mesh stiffness variation and clearance non-linearity has been studied by Kahraman and Blankenship [19, 20] for single-mesh gears. The effects on multi-mesh planetary gears need additional investigation.

6. CONCLUSIONS

This work analytically investigates the parametric instabilities from mesh stiffness variation in planetary gears. Instability boundaries are obtained for systems with equally spaced (summarized in Table 2) and diametrically opposed planets. The main points are:

(1) Using the structured properties of vibration modes, the instability boundaries are reduced to simple, closed-form expressions for several planet-phasing conditions. The instability boundaries are sensitive to contact ratios and mesh phasing, and the simple expressions are useful in design to suppress instabilities by adjusting these parameters.
(2) Certain parametric instabilities always vanish for particular mesh-phasing conditions, including (1) combination instabilities of distinct and degenerate modes when equally spaced planets are in-phase, (2) primary and combination instabilities of distinct modes when equally spaced planets are sequentially phased, and (3) primary and combination instabilities of distinct modes when diametrically opposed planets are counter-phased. These features come from the well-defined modal properties and apply to any form of mesh stiffness variation.
(3) Instability boundaries relate directly to mesh deformations in the vibration modes. The mesh parameters (e.g., c_s and c_r) that are most critical to a particular instability are those of the tooth meshes with dominant deformations in the unstable vibration modes.
(4) When a parametric instability is excited under operating condition's, tooth separation occurs. This non-linearity dramatically changes the dynamic response. More analysis is needed to reveal the interaction of mesh stiffness variation and backslash non-linearity in multi-mesh gear systems.

ACKNOWLEDGMENTS

The authors would like to thank Timothy L. Krantz of the Army Research Lab at NASA Glenn Research Center for his support and advice on the project. This material is based upon work supported by the U.S. Army Research Office under grant DAAD19-99-1-0218.

REFERENCES

1. M. BENTON and A. SEIREG 1978 *Journal of Mechanical Design* **100**, 26–30. Simulation of resonances and instability conditions in pinion–gear systems.
2. J. G. BOLLINGER and R. J. HARKER 1967 *Journal of the Industrial Mathematics* **17**, 39–55. Instability potential of high speed gearing.
3. M. BENTON and A. SEIREG 1981 *Journal of Mechanical Design* **103**, 372–378. Factors influencing instability and resonances in geared systems.
4. C. NATARAJ and N. K. ARAKERE 1999 *American Society for Mechanical Engineers Design Engineering Technical Conferences, Paper No. DETC99/VIB*-8110, *September, Las Vegas, NV*. Dynamics response and stability of a spur gear pair.

5. M. AMABILI and A. RIVOLA 1997 *Mechanical Systems and Signal Processing* **11**, 375–390. Dynamic analysis of spur gear pairs: steady-state response and stability of the sdof model with time-varying meshing damping.
6. C. NATRAJ and A. M. WHITMAN 1997 *American Society for Mechanical Engineers Design Engineering Technical Conferences*, *Paper No. DETC*97/*VIB*-4018, *September*, *Sacramento*, *CA*. Parameter excitation effects in gear dynamics.
7. G. V. TORDION and R. GAUVIN 1977 *Journal of Engineering for Industry* **99**, 785–791. Dynamic stability of a two-stage gear train under the influence of variable meshing stiffnesses.
8. M. BENTON and A. SEIREG 1980 *Journal of Mechanical Design* **102**, 379–383. Normal mode uncoupling of systems with time varying stiffness.
9. J. LIN and R. G. PARKER 2001 *Journal of Vibration and Acoustics* **124**. Mesh stiffness variation instabilities in two-stage gear systems.
10. R. AUGUST and R. KASUBA 1986 *Journal of Vibration*, *Acoustics*, *Stress*, *and Reliability in Design* **108**, 348–353. Torsional vibrations and dynamic loads in a basic planetary gear system.
11. P. VELEX and L. FLAMAND 1996 *Journal of Mechanical Design* **118**, 7–14. Dynamic response of planetary trains to mesh parametric excitations.
12. J. LIN and R. G. PARKER 1999 *Journal of Vibration and Acoustics* **121**, 316–321. Analytical characterization of the unique properties of planetary gear free vibration.
13. J. LIN and R. G. PARKER 2000 *Journal of Sound and Vibration* **233**, 921–928. Structural vibration characteristics of planetary gears with unequally spaced planets.
14. D. L. SEAGER 1975 *Journal of Mechanical Engineering Science* **17**, 293–298. Conditions for the neutralization of excitation by the teeth in epicyclic gearing.
15. A. KAHRAMAN and G. W. BLANKENSHIP 1994 *Proceedings of the International Gearing Conference*, *Newcastle*, *U.K.*, 99–104. Planet mesh phasing in epicyclic gear sets.
16. A. KAHRAMAN 1994 *Journal of Mechanical Design* **116**, 713–720. Planetary gear train dynamics.
17. R. G. PARKER 2000 *Journal of Sound and Vibration* **236**, 561–573. A physical explanation for the effectiveness of planet phasing to suppress planetary gear vibration.
18. R. KASUBA and J. W. EVANS 1981 *Journal of Mechanical Design* **103**, 398–409. An extended model for determining dynamic loads in spur gearing.
19. A. KAHRAMAN and G. W. BLANKENSHIP 1996 *Journal of Sound and Vibration* **194**, 317–336. Interactions between commensurate parametric and forcing excitations in a system with clearance.
20. A. KAHRAMAN and G. W. BLANKENSHIP 1997 *Journal of Applied Mechanics* **64**, 217–226. Experiments on nonlinear dynamic behavior of an oscillator with clearance and periodically time-varying parameters.